Molecular Neurobiology (2019) 56:4464–4478
https://doi.org/10.1007/s12035-018-1393-1

Laquinimod Treatment Improves Myelination Deficits at the Transcriptional and Ultrastructural Levels in the YAC128 Mouse Model of Huntington Disease

Marta Garcia-Miralles[1] · Nur Amirah Binte Mohammad Yusof[1] · Jing Ying Tan[1] · Carola I. Radulescu[1] · Harwin Sidik[1] · Liang Juin Tan[1] · Haim Belinson[2] · Neta Zach[2] · Michael R. Hayden[1,2,3,4] · Mahmoud A. Pouladi[1,4]

Received: 5 September 2018 / Accepted: 11 October 2018 / Published online: 17 October 2018

Abstract

Laquinimod, an immunomodulatory agent under clinical development for Huntington disease (HD), has recently been shown to confer behavioural improvements that are coupled with prevention of atrophy of the white matter (WM)-rich corpus callosum (CC) in the YAC128 HD mice. However, the nature of the WM improvements is not known yet. Here we investigated the effects of laquinimod on HD-related myelination deficits at the cellular, molecular and ultrastructural levels. We showed that laquinimod treatment improves motor learning and motor function deficits in YAC128 HD mice, and confirmed its antidepressant effect even at the lowest dose used. In addition, we demonstrated for the first time the beneficial effects of laquinimod on myelination in the posterior region of the CC where it reversed changes in myelin sheath thickness and rescued *Mbp* mRNA and protein deficits. Furthermore, the effect of laquinimod on myelin-related gene expression was not region-specific since the levels of the *Mbp* and *Plp1* transcripts were also increased in the striatum. Also, we did not detect changes in immune cell densities or levels of inflammatory genes in 3-month-old YAC128 HD mice, and these were not altered with laquinimod treatment. Thus, the beneficial effects of laquinimod on HD-related myelination abnormalities in YAC128 HD mice do not appear to be dependent on its immunomodulatory activity. Altogether, our findings describe the beneficial effects of laquinimod treatment on HD-related myelination abnormalities and highlight its therapeutic potential for the treatment of WM pathology in HD patients.

Keywords Huntington disease · Behaviour · Laquinimod · White matter · Oligodendroglia · Myelination

Introduction

Huntington disease (HD) is an inherited, progressive neurodegenerative disorder caused by a CAG repeat expansion in exon 1 of the huntingtin (*HTT*) gene [1]. Clinically, HD is characterised by a triad of symptoms which include psychiatric disturbances such as depression and psychosis, cognitive deficits and motor function impairment [1]. The neuropathological phenotypes of HD include degeneration of the caudate putamen and thinning of the cortex as well as early and progressive atrophy of white matter structures [1–5]. No effective therapies are currently available to prevent, slow down, or reverse the progression of HD.

Studies in patients as well as mouse models of HD have provided increasing evidence of a role for abnormal immune activation as an early disease event in HD [2–12]. Profiling of serum inflammatory markers has revealed abnormalities in immune activation as early as 16 years prior to clinical onset in premanifest mutation carriers, and at 9–12 months of age in

Electronic supplementary material The online version of this article (https://doi.org/10.1007/s12035-018-1393-1) contains supplementary material, which is available to authorized users.

✉ Mahmoud A. Pouladi
pouladi@tlgm.a-star.edu.sg; map@pouladilab.org

[1] Translational Laboratory in Genetic Medicine, Agency for Science, Technology and Research, Singapore (A*STAR), 8A Biomedical Grove, Immunos, Level 5, Singapore 138648, Singapore

[2] Teva Pharmaceutical Industries Ltd, Research and Development, Netanya, Israel

[3] Centre for Molecular Medicine and Therapeutics, Child and Family Research Institute, University of British Columbia, Vancouver, BC V5Z 4H4, Canada

[4] Department of Medicine, Yong Loo Lin School of Medicine, National University of Singapore, Singapore 117597, Singapore

the YAC128 mouse model of HD [6, 7]. Also, some of the reported observations such as widespread microglial activation and elevated levels of proinflammatory immune factors in cerebrospinal fluid and plasma samples have been shown to correlate with disease progression [2, 6–13] supporting their utility as potential biomarkers of disease progression as well as possible targets for therapeutic intervention.

Laquinimod is a novel immunomodulatory agent in clinical development for HD. Although its precise mechanism(s) of action have not been fully elucidated [13, 14], laquinimod has been shown to modulate the peripheral innate immune system as well as distinct cell populations resident in the central nervous system (CNS), especially astrocytes and microglia [5, 14–16]. In addition to its anti-inflammatory properties, laquinimod has been shown to be neuroprotective, upregulating BDNF [5, 15, 16] and also reducing demyelination and axonal damage in mouse models of neuroinflammatory diseases such as multiple sclerosis (MS) [14, 15]. A major mediator of laquinimod's immunomodulatory effects has been shown to be the aryl hydrocarbon receptor (AhR) pathway [14, 17]. However, the mechanisms of its neuroprotective effects and whether immunomodulation is the primary or sole mechanism of laquinimod's beneficial effects on myelination remain unclear.

We have recently shown that laquinimod treatment rescues striatal, cortical and callosal atrophy, and improves in imaging-based measures of white matter (WM) integrity in a dose-specific manner in the YAC128 mouse model of HD [17–19]. Here, we sought to examine the effect of lower doses of laquinimod on behavioural outcomes, as well as to investigate the nature of the improvements on WM at the cellular, molecular and ultrastructural levels. We demonstrate that low doses of laquinimod improved some behavioural outcomes, such as motor learning, motor function and depression, and reversed changes in myelin thickness in the corpus callosum (CC) of YAC128 HD mice. In addition, we observed that ultrastructural myelin-related alterations were accompanied by an increase in *Mbp* gene expression but were not associated with changes in the number of oligodendroglia. Our findings provide insights into the nature of the WM improvements induced by laquinimod in HD, and offer further evidence of the beneficial effects of laquinimod on white matter microstructures.

Material and Methods

Animals Male and female YAC128 HD mice (line 53) expressing a full-length human *HTT* transgene with 128 CAG repeats and WT mice maintained on the FVB/N strain were used [18, 19]. Mice were bred at the Biological Resource Centre (Agency for Science, Technology and Research, ASTAR), and housed in individually ventilated cages in groups of two to five mice with littermates on a 12-h light cycle (lights on at 09:00). Food (Altromin 1324 irradiated modified 18% protein and 6% fat) and water were provided ad libitum. Experiments were performed with the approval of the Institutional Animal Care and Use Committee (IACUC # 151067) at the Biomedical Sciences Institute (ASTAR) and in accordance with their approved guidelines.

Administration of Laquinimod Laquinimod was synthesised by Teva Pharmaceutical Industries and was dissolved in sterile water. Laquinimod and vehicle were administered by oral gavage daily starting at 5 weeks of age, for a period of 7 weeks. Mice received vehicle (sterile water), 0.25 mg/kg of laquinimod or 1 mg/kg of laquinimod at a volume of 4 mL/kg. Animals were weighed every 2 weeks to ensure the correct dose was maintained.

Study Design Laquinimod was administered to three independent cohorts of animals in the early stages of disease (5 weeks of age). For all cohorts, animals were identified by earmarks and divided into four groups randomly. Two groups of YAC128 HD mice received laquinimod at a dose of 0.25 or 1 mg/kg, whereas the remaining groups, WT and YAC128 HD mice received an equivalent volume of vehicle (sterile water) (Fig. 1). For the behavioural cohort (independent cohort 1; for all groups: $N = 13–14$; 6–7 females/7–8 males), a battery of behavioural tests was performed in mice between 11 and 12 weeks of age in the following order: rotarod training (motor learning), accelerating rotarod (motor function), climbing test (motor function) and Porsolt forced swim test (psychiatric function) (Fig. 1). All behavioural tests were performed during the dark phase of the light cycle and mice were acclimated to the room for at least 30 min before the beginning of each test. Animals from the behavioural cohort were euthanized following completion of behavioural testing at 13 weeks of age for stereological analysis of glial populations (Fig. 1). For white matter pathology assessment, two independent cohorts of mice were euthanized at 12 weeks of age for myelin sheath analysis (cohort 2; for all groups: $N = 4$, all males) or mRNA analysis (cohort 3; for all groups: $N = 6$; all males) (Fig. 1).

Motor Learning and Accelerating Rotarod Test The rotarod training is used to assess cognitive motor learning function in rodents (UGO Basile 47600 Rotarod, rotating rod diameter 3 cm) [17–19]. Training was carried out at 11 weeks of age and consisted of three trials (120 s each) per day, spaced 1 h apart, at a fixed speed of 18 rpm for three consecutive days. The rotarod test is designed to evaluate motor coordination and balance in rodents. The testing phase was also carried out at 11 weeks of age, and consisted of three trials, spaced 2 h apart. During each trial the rotarod accelerated from 5 to 40 rpm over 5 min. Rotarod scores are the average of three trials.

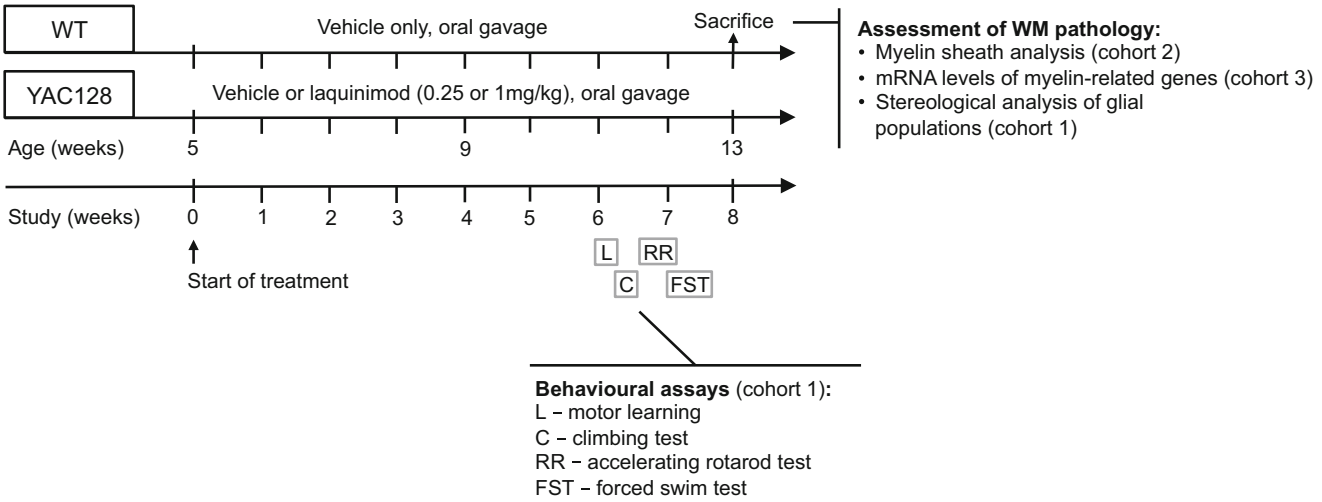

Fig. 1 Schematic representation of the experimental design. WT mice were administered vehicle (ddH_2O) only, whereas YAC128 HD mice were administered either vehicle (ddH_2O) or laquinimod (0.25 or 1 mg/kg). Treatment started at 5 weeks of age and continued for 7 weeks. Three independent cohorts of animals were used for behavioural and/or white matter (WM) pathology assessment. Behavioural tests were carried out in cohort 1 as indicated: L = motor learning, RR = accelerating rotarod, C = climbing test, FST = forced swim test. All mice were sacrificed at 12–13 weeks of age

Climbing Test The climbing test is used to assess motor function in rodents [17, 19]. Each trial session consisted of an acclimatisation phase and a test phase. In the acclimatisation phase, mice were allowed to acclimatise to the testing room for at least 30 min before testing. In the test phase, mice were placed at the bottom end of a closed-top wire-mesh cylinder and their behaviour was recorded for 5 min. Time spent climbing and the latency to climb were the two variables used to assess motor performance in each mouse. Time spent climbing was scored when all four paws of a mouse left the table top to the time when the first paw was placed back on the table top. For each mouse, the sum of the time spent climbing for the 5-min trial (total time climbing) and the latency of each mouse to start climbing (latency to climb) were scored. An investigator blinded to genotype and treatment group performed the video scoring.

Porsolt Forced Swim Test of Depression The Porsolt forced swim test (FST) was performed as described previously [20]. Briefly, mice were placed in individual cylinders (25 cm tall × 19 cm wide) filled with room temperature water (23–25 °C) to a depth of 15 cm for a period of 6 min. The test sessions were recorded by a video camera placed directly above the cylinders by a non-blinded investigator. The last 4 min of the test session was scored using a time-sampling technique to rate the predominant behaviour over 5-s intervals. The following behaviours were measured at the end of every 5 s: swimming/climbing and immobility. An investigator blinded to genotype and treatment group performed the video scoring.

Brain Sample Preparation for Histology Mice were anaesthetised with intraperitoneal injections of ketamine (150 mg/kg) and xylazine (10 mg/kg) mixture. For histology, animals were perfused at 13 weeks of age with ice-cold phosphate-buffered saline (PBS) followed by ice-cold 4% paraformaldehyde (PFA) in PBS. Brains were removed and left in 4% PFA for 24 h. The following day, brains were washed in PBS, transferred into a 30% sucrose solution containing 0.08% sodium azide in PBS and kept at 4 °C until used. For sectioning, brains were frozen on dry ice with isopentane, mounted with Tissue-TEK O.C.T. compound (Sakura, Torrance, CA, USA), and sliced coronally into 25-μm sections on a cryostat (Microm HM 525, Thermo-Fisher Scientific, Waltham, MA, USA). The sections were collected and stored in PBS with 0.08% sodium azide at 4 °C until use.

Immunohistofluorescence A series of 25-μm thick coronal sections spanning the corpus callosum were treated for antigen retrieval with 1 M hydrochloric acid (HCl) at 4 °C, 2 M HCl at room temperature, 2 M HCl at 37 °C and borate buffer (pH 9) at room temperature. Sections were then incubated in 5% donkey or goat serum and 0.2% Triton X-100 in PBS, and subsequently sections were stained with goat anti-PDGFRα (1:200; R&D Systems, AF1062) or rabbit anti-Olig2 (1:750; Merck KGaA, AB9610) antibodies overnight at room temperature, respectively. Following a wash with PBS, sections were incubated with donkey anti-goat Alexa-488 and goat anti-rabbit Alexa-555 secondary antibodies (1:500; Thermo-Fisher Scientific, A-11055, and A-21428, respectively) for 2 h at room temperature. Following a final wash with PBS, sections were mounted on slides and cover slipped with Fluoromount™ mounting medium (Merck KGaA). Validation data for each antibody is available from the respective company.

Immunohistochemistry A series of 25-μm thick coronal sections spanning the corpus callosum were incubated with rabbit anti-GSTpi (1:1000; MBLI, #311), rabbit anti-Iba1 (1:1000; Wako, #019-19741) or rabbit anti-GFAP antibodies (1:500; Merck KGaA, AB5804) overnight at 4 °C in 5% normal goat serum (NGS) and 0.2% Triton X-100 in PBS, followed by incubation with biotinylated anti-rabbit antibody (1:200; Vectastain ABC HRP Kit, PK-4006; Vector Laboratories, Burlingame, CA, USA) for 1.5 h at room temperature with 1% NGS, 0.2% Triton X-100 in PBS. After three washes in PBS, sections were incubated in Vectastain Elite ABC reagent (Vector Labs Inc., Burlingame, CA, USA) for 2 h at room temperature and staining was visualised using 3,3′-diaminobenzidine (DAB) (ImmPACT DAB Peroxidase Substrate, SK-4105; Vector Laboratories, Burlingame, CA, USA). Sections were mounted on slides and cover slipped with DPX mounting media (Sigma, 44581). Validation data for each antibody is available from the respective company.

Stereological Measurements Number of PDGFRα-, Olig2-, GSTpi-, GFAP- and Iba1-positive cells in the corpus callosum as well as the area of the corpus callosum were determined by examining six to nine coronal sections per mouse at 300-μm intervals covering the corpus callosum (both hemispheres). Analysis was done using the Stereo Investigator Software (MBF Bioscience, Williston, VT, USA) with optical fractionator (cells counts) or Cavalieri probe (area) connected to an AxioImager M2 microscope (Carl Zeiss AG, Oberkochen, Germany) and AxioCam MRc Digital CCD camera (Carl Zeiss AG, Oberkochen, Germany). The following parameters were used: 150 × 150 μm counting frame size and 450 × 450 μm grid size for GFAP and Iba1, 50 × 50 μm counting frame size and 300 × 300 μm grid size for GSTpi, 100 × 100 μm counting frame size and 450 × 450 μm grid size for Olig2, and 150 × 150 μm counting frame size and 350 × 450 μm grid size for PDGFRα. For all stereological measurements, a 10-μm dissector height and 5 μm guard were used. For all analysis, investigator was blinded to genotype and treatment. Representative images for all stainings were acquired using a Ni-E microscope (Nikon Corporation) and DS-Ri2 colour camera (Nikon Corporation).

Brain Sample Preparation for Transmission Electron Microscopy For transmission electron microscopy (TEM), animals from cohort 2 were perfused at 12 weeks of age with ice-cold PBS followed by ice-cold 2.5% PFA and 2.5% glutaraldehyde (GlutAH) in PBS. Brains were removed and left in 2.5% PFA and 2.5% GlutAH for 24 h, washed in PBS and then transferred to a 5% sucrose solution containing 0.08% sodium azide in PBS at 4 °C until use.

Transmission Electron Microscopy A coronal slice of 1 mm was made at the intersection between the CC and fornix using a mouse brain stainless steel matrix (Roboz Surgical Instrument Company). According to the mouse brain atlas [21], the anterior region of the CC (from bregma 1.10 to 0.50 mm) and the posterior region of the CC (from bregma − 1.82 to − 2.70) [22] were microdissected before post-fixation in 1% osmium tetroxide for 1 h at room temperature. After washing twice in deionised water, samples were dehydrated, infiltrated with acetone and resin, embedded and polymerised at 60 °C for 24 h. Ultra-thin slices (90 nm) were sectioned before imaging on a transmission electron microscope. Samples were viewed using a Tecnai G2 Spirit Twin/Biotwin model (FEI, USA) and 10–12 images were taken from each animal. Images were taken by an investigator blinded to genotype and treatment.

G-Ratio Analysis A total of 12 images per animal were analysed using ImageJ software (version 2.0.0). An unbiased frame was randomly selected and superimposed on each image. Within the selected region of interest, the axonal diameter (ID) and outer diameter (OD) of regular shaped and myelinated axons was measured and the g-ratio was calculated. Approximately a total of 100 to 600 axons per animal were measured for the anterior as well as posterior region of the corpus callosum analysis. G-ratio analysis was performed by an investigator blinded to genotype and treatment.

Brain Tissue Collection for Molecular Analysis Striata and corpora callosa from animals from cohort 3 were dissected at 12 weeks of age, snap-frozen in liquid nitrogen and stored at − 80 °C until use.

RNA Extraction and Quantitative Real-Time PCR Tissues were lysed using Trizol and chloroform, and RNA was purified using the FARB mini column (Favorgen) according to the manufacturer's instructions. For all samples, cDNA was generated using SuperScript™ II Reverse Transcriptase (Life Technologies). Quantitative real-time PCR was run on the QuantStudio 6 Flex Real-Time PCR System (Applied Biosystems) using primers listed in Table 1. Relative gene expression levels were analysed using the Comparative CT Method (ΔΔCT Method).

Immunoblotting Protein lysate of corpora callosa from female mice were prepared using RIPA buffer (Sigma-Aldrich) with 1 mM PMSF (Sigma-Aldrich), 5 μm Z-VAD (Promega), 1 mM NaVan (Sigma-Aldrich) and 1× Complete Protease Inhibitor Cocktail tablets (Roche). For immunoblotting, 20 μg of protein lysates was separated on 12% Bis-Tris protein gel (Novex) with 20× MES running buffer (Novex). Samples were transferred onto nitrocellulose membranes, blocked with Odyssey Blocking Buffer (*LI-COR*, P/N 927-40000) 1 h at room temperature, and then incubated with primary antibodies rat anti-MBP (1:1000; Millipore, MAB5680) and mouse anti-Calnexin

Table 1 Primers used for qRT-PCR analysis

Target (mouse)	Forward primer (5′ → 3′)	Reverse primer (5′ → 3′)
Mbp	GGCCAGTAAGGATGGAGAGAT	CCTCTGAGGCCGTCTGAGA
Plp1	GAGGCCAACATCAAGCTCAT	CCAACTTGTCGGGATGTCCT
Ermn	CTGAGACACTGAGCGGGAC	CAACCTTGTAGTATGCCTGGG
Cnp	TTTACCCGCAAAAGCCACACA	CACCGTGTCCTCATCTTGAAG
Mog	AGCTGCTTCCTCTCCCTTCTC	ACTAAAGCCCGGATGGGATAC
Il6	TAGTCCTTCCTACCCCAATTTCC	TTGGTCCTTAGCCACTCCTTC
Il1b	GCAACTGTTCCTGAACTCAACT	ATCTTTTGGGGTCCGTCAACT
Tnfa	CCCTCACACTCAGATCATCTTCT	GCTACGACGTGGGCTACAG
Cyp1A1	CCTCTTTGGAGCTGGGTTTG	TGCTGTGGGGGATGGTGA
β-actin	GGCTGTATTCCCCTCCATCG	CCAGTTGGTAACAATGCCATGT

(1:10000; Sigma-Aldrich, C4731) overnight at 4 °C. Membranes were then incubated with secondary antibodies Alexa-Fluor goat anti-rat 680 (1:10,000; Thermo-Fisher Scientific, A21096) and Alexa-Fluor goat anti-rabbit 800 (1:10,000; Thermo-Fisher Scientific, A32735) 2 h at room temperature. The membrane was imaged using the *LI-COR* Imaging System and Odyssey V3.0 software (*LI-COR*).

Statistical Analysis Unless otherwise stated, comparisons between treatment groups were assessed using a one-way ANOVA with Fisher's LSD post hoc analysis. Where indicated, pair-wise comparisons between groups at individual time points were assessed with Student's *t* test or Kolmogorov-Smirnov test. Outliers identified by Grubbs' test (alpha < 0.05) were excluded from the analysis. GraphPad Prism v6 software was used to analyse data for statistical significance. Differences were considered statistically significant when $p < 0.05$.

Results

Laquinimod Improves Motor Learning and Depressive Behaviour in YAC128 HD Mice

We have previously shown that laquinimod treatment (1 and 10 mg/kg) rescues striatal, cortical and white matter pathology and results in improvements in motor function and depressive-like behaviour in the YAC128 mouse model of HD [17]. Since most of the HD-related phenotypes rescued by laquinimod were observed with the 1 mg/kg dose, we sought to further explore the effects of laquinimod when given at an even lower dose (0.25 mg/kg) as well as when administered prior to the onset of disease-related phenotypes in the YAC128 HD mice (5 weeks of age).

We first examined the effect of laquinimod on motor learning. Consistent with previous studies, vehicle-treated YAC128 exhibited motor learning deficits compared with vehicle-treated WT mice as signified by a reduced latency to fall at 11 weeks of age (Fig. 2a; one-way ANOVA: $p = 0.0113$ at day 1, $p = 0.0073$ at day 2, $p = 0.0432$ at day 3; Fisher's LSD post hoc analysis: $p < 0.05$ at day 1, $p > 0.05$ at day 2 and $p < 0.01$ at day 3) [18, 23]. Motor learning function of YAC128 HD mice was improved with the lowest dose of laquinimod treatment (0.25 mg/kg) to levels not significantly different from that of vehicle-treated WT mice at day 1 of training (Fig. 2a; one-way ANOVA: $p = 0.0113$ at day 1; Fisher's LSD post hoc analysis: $p > 0.05$), whereas both doses partially rescued motor learning function of YAC128 HD mice compared with vehicle-treated WT mice at day 3 of training (Fig. 2a; one-way ANOVA: $p = 0.0432$ at day 3; Fisher's LSD post hoc analysis: *n.s.* for both doses compared with vehicle-treated WT mice).

Next, mice were assessed on the accelerating rotarod task and the climbing test to evaluate their motor function. In agreement with previous studies, vehicle-treated YAC128 HD mice exhibited motor performance deficits compared with vehicle-treated WT mice in the accelerating rotarod task at 3 months of age (Fig. 2b; one-way ANOVA: $p = 0.1479$; paired Student's *t* test, $p < 0.05$) [17, 18, 23–25]. Laquinimod treatment at 1 mg/kg improved motor function in the accelerating rotarod task to levels not significantly different from that of vehicle-treated WT mice (Fig. 2b; one-way ANOVA: $p = 0.1479$) as previously shown [17], whereas 0.25 mg/kg of laquinimod did not improve motor function in YAC128 HD mice compared with vehicle-treated YAC128 HD mice (Fig. 2b; one-way ANOVA: $p = 0.1479$).

In the climbing test, no deficits were observed in vehicle-treated YAC128 HD mice compared with vehicle-treated WT mice (Fig. 2c; one-way ANOVA: $p = 0.8483$). This finding is consistent with previous reports, which show that YAC128 HD mice do not display a very robust climbing deficit at 3 months of age [17]. Treatment with laquinimod (0.25 and 1 mg/kg) had no effect on climbing performance in YAC128 HD mice (Fig. 2c; one-way ANOVA: $p = 0.8483$).

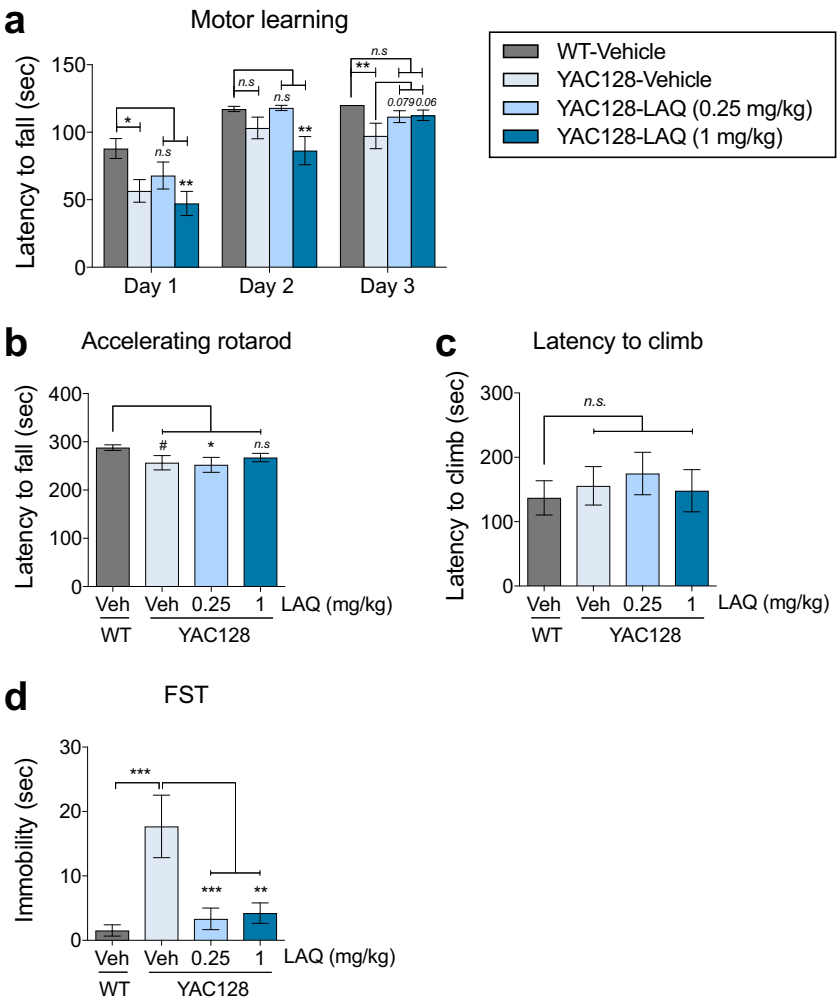

Fig. 2 Effect of laquinimod treatment on HD-related behavioural phenotypes in YAC128 mice. Vehicle-treated YAC128 HD mice displayed motor learning deficits compared to vehicle-WT mice (**a**). Low dose of laquinimod (0.25 mg/kg) improved motor learning deficits at day 1 of training by increasing the latency to fall in YAC128 HD mice, whereas both doses (0.25 and 1 mg/kg) partially rescued motor learning deficits at day 3 of training (**a**). There was no effect of high dose laquinimod (1 mg/kg) on motor learning in YAC128 HD mice on days 1 and 2 (**a**). In addition, vehicle-treated YAC128 HD mice showed motor deficits in the accelerating rotarod (**b**) but not in the climbing test (**c**). Laquinimod treatment (1 mg/kg) partially improved motor performance in the accelerating rotarod test (**b**), but no effect of laquinimod was observed in the climbing test (**c**). Also, vehicle-treated YAC128 HD mice exhibited depression-like phenotype, which was reduced by laquinimod treatment as signified by a decrease in immobility (**d**). Values shown as mean ± SEM; $*p < 0.05$, $**p < 0.01$, $***p < 0.001$ by one-way ANOVA with Fisher's LSD post hoc analysis; $^{\#}p < 0.05$ by paired Student's *t* test; $N = 11–14$ per genotype/group (females and males); Veh = vehicle; LAQ = laquinimod; FST = forced swim test

Finally, the effect of laquinimod on depressive-like behaviour was assessed using the Porsolt FST. At 3 months of age, vehicle-treated YAC128 HD mice displayed depressive-like phenotype in the FST as shown by increased immobility time compared with vehicle-treated WT mice, confirming previous reports [17, 20] (Fig. 2d; one-way ANOVA: $p = 0.0004$; Fisher's LSD post hoc analysis: $p < 0.001$). Both doses of laquinimod treatment reduced immobility time in YAC128 HD mice, improving depressive-like phenotype (Fig. 2d; one-way ANOVA: $p = 0.0004$; Fisher's LSD post hoc analysis: $p < 0.001$ for 0.25 mg/kg and $p < 0.01$ for 1 mg/kg of laquinimod). Altogether, these findings suggest that low doses of laquinimod treatment (0.25 and 1 mg/kg) result in improvements in motor learning phenotypes, and validate the beneficial effects of laquinimod on motor function (accelerating rotarod) and depressive-like phenotype in YAC128 HD mice [17].

No Effect of Laquinimod on Cell Densities of Oligodendroglia, Microglia or Astrocytes in Young YAC128 HD Mice

YAC128 HD mice have been shown to present myelination abnormalities in the CC [26, 27], and laquinimod treatment partially rescued aspects of these deficits [17]. To determine whether the effect of laquinimod on myelination abnormalities is due to an effect on glial cells, we first investigated the number

of oligodendrocytes, the myelinating cells of the CNS, and their precursors by immunohistochemistry and stereology in vehicle-treated WT and YAC128 HD mice at 3 months of age (Fig. 3a). Overall, no differences in cell density of oligodendroglial progenitor cells (PDGFRα$^+$), pre-myelinating oligodendrocytes (Olig2$^+$) and myelinating oligodendrocytes (GSTpi$^+$) were observed in vehicle-treated YAC128 HD mice compared with vehicle-treated WT mice (Fig. 3b–d; one-way ANOVA: $p = 0.7950$ for PDGFRα, $p = 0.8839$ for Olig2, $p = 0.6056$ for GSTpi). Laquinimod treatment did not have any effect on cell density of these three oligodendroglial populations in the CC of YAC128 HD mice (Fig. 3b–d; one-way ANOVA: $p = 0.7950$ for PDGFRα, $p = 0.8839$ for Olig2, $p = 0.6056$ for GSTpi).

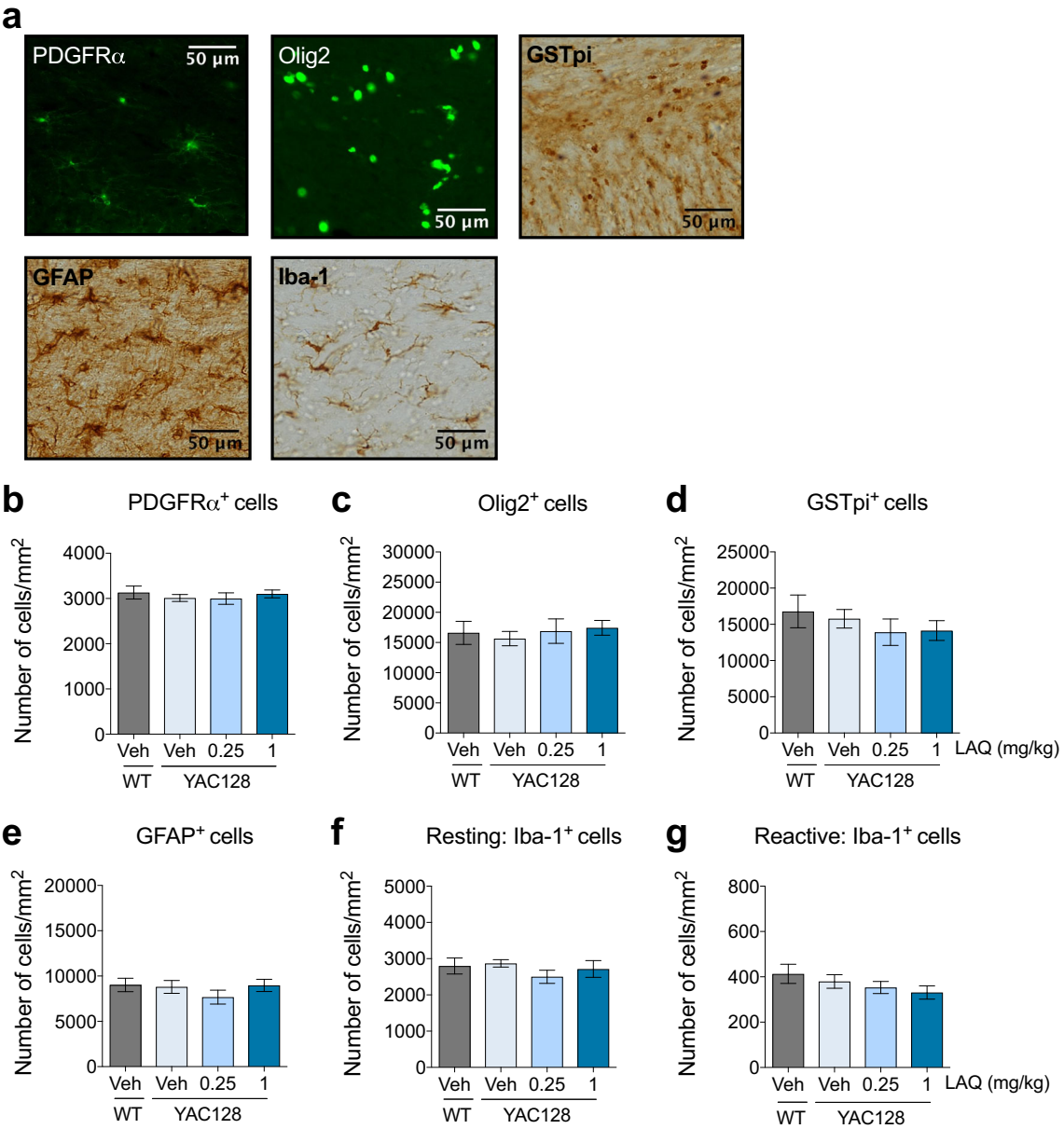

Fig. 3 No effect of laquinimod on cell densities of oligodendroglia, microglia or astrocytes in the corpus callosum of young YAC128 HD mice. Representative images of PDGFRα$^+$, Olig2$^+$, GSTpi$^+$, GFAP$^+$ and Iba-1$^+$ stainings in the corpus callosum (CC). Scale bar = 50 µm (**a**). Vehicle-treated YAC128 HD mice did not present changes in cell density of oligodendroglia precursor cells (PDGFRα$^+$) (**b**), pre-myelinating oligodendrocytes (Olig2$^+$) (**c**), myelinating oligodendrocytes (GSTpi$^+$) (**d**), astrocytes (GFAP$^+$) (**e**) or microglial cells (Iba-1$^+$) both resting (**f**) and reactive (**g**) in the corpus callosum compared with vehicle-treated WT mice at 3 months of age. Laquinimod treatment did not have any effect on the cell density of these glial populations (**b**–**g**). Values shown as mean ± SEM; *n.s.* by one-way ANOVA with Fisher's LSD post hoc analysis; $N = 9$–11 per genotype/group (females and males). Veh = vehicle; LAQ = laquinimod; PDGFRα$^+$ = platelet-derived growth factor receptor; Olig2$^+$ = oligodendrocyte transcription factor; GSTpi$^+$ = glutathione S-transferase pi 1; GFAP$^+$ = glial fibrillary acidic protein; Iba1$^+$ = ionised calcium-binding adapter molecule 1

Because laquinimod has been shown to act on astrocytes and microglia, reducing these two glial populations and their activation under inflammatory conditions [28], we also assessed the cell density of these two cell types in the CC (Fig. 3a). We observed no differences in the cell density of astrocytes ($GFAP^+$) or microglia ($Iba1^+$) in vehicle-treated YAC128 HD mice compared with vehicle-treated WT mice (Fig. 3e–g; one-way ANOVA: $p = 0.5456$ for GFAP, $p = 0.5784$ for Iba-1 resting, $p = 0.3449$ for Iba-1 reactive), suggesting no overt inflammatory response in YAC128 HD mice under baseline conditions at this young age. Laquinimod treatment had no effect on the cell density of these two glial populations in YAC128 HD mice compared with vehicle-treated YAC128 HD mice (Fig. 3e–g; one-way ANOVA: $p = 0.5456$ for GFAP, $p = 0.5784$ for Iba-1 resting, $p = 0.3449$ for Iba-1 reactive). Taken together, these findings suggest that WM improvements previously observed in YAC128 HD mice treated with laquinimod [17] likely result from a mechanism that does not change glial cell numbers, but modifies intrinsic cellular properties.

Laquinimod Reverses HD-Related Changes in Myelin Sheath Thickness in the Posterior Region of the CC in YAC128 HD Mice

To examine the effect of laquinimod on myelin ultrastructure, we calculated the g-ratios of myelinated axons in the anterior and posterior regions of the CC on images obtained by transmission electron microscopy (Fig. 4a). As shown in the diagram in Fig. 4b, the g-ratio is calculated as the ratio between the axonal diameter, also referred as inner diameter (ID) or calibre, and the outer diameter (OD) of myelinated axons. Consistent with our previous findings [27], g-ratios were on average higher in vehicle-treated YAC128 HD mice compared with vehicle-treated WT mice at 3 months of age in the anterior region of the CC as signified by the slope of the best-fit line in the scatter plot of g-ratio versus axonal diameters (Fig. 4c; left panel; $p = 0.0026$), which also suggests that axons with a diameter below 0.5 μm mainly account for this higher g-ratio. Cumulative frequency analysis corroborates this observation, showing that g-ratios for axons with a calibre below 0.5 μm are significantly higher in vehicle-treated YAC128 HD mice compared with vehicle-treated WT mice (Fig. 4d; left panel; Kolmogorov-Smirnov test, $p < 0.001$) whereas those for axons with a calibre of 0.5 μm or higher are not different between the genotypes (Fig. 4d; right panel; Kolmogorov-Smirnov test, $p = 0.1319$). When we examined the effect of laquinimod treatment on this part of the CC, we did not observe any differences on myelin thickness with the lower dose of laquinimod in axons with a calibre below 0.5 μm, as the best-fit line from the scatter plot and the cumulative frequencies were not different between vehicle- and laquinimod-treated YAC128 HD mice (Fig. 4c; middle panel; slope $_{[\text{vehicle-treated YAC128}]} = 0.2103 \pm 0.0075$, slope $_{[0.25\ \text{mg/kg laquinimod-treated YAC128}]} = 0.2292 \pm 0.0081$, $p = 0.0906$; Fig. 4d; left panel; Kolmogorov-Smirnov test, $p = 0.6083$). However, the cumulative frequency of g-ratios in axons with a calibre above 0.5 μm revealed that the low dose of laquinimod increased the g-ratio of myelinated axons compared with vehicle-treated YAC128 HD mice, suggesting that laquinimod decreases myelin thickness or increases myelin compaction in the anterior region of the CC of YAC128 HD mice (Fig. 4d; right panel; Kolmogorov-Smirnov test, $p < 0.05$). We did not observe any changes on myelin thickness with the higher dose of laquinimod (Fig. 4c; right panel; slope $_{[\text{vehicle-treated YAC128}]} = 0.2103 \pm 0.0075$, slope $_{[1\ \text{mg/kg laquinimod-treated YAC128}]} = 0.1984 \pm 0.0077$, $p = 0.2706$; Fig. 4d; left and right panels; Kolmogorov-Smirnov test, $p > 0.05$).

Because we previously observed improvements in white matter structures using magnetic resonance imaging-based measures in the posterior region of the CC following laquinimod treatment [17], we also assessed changes in myelin sheath thickness in this region of the CC. Examination of the scatter plot analysis of g-ratios versus axonal diameters revealed differences in g-ratios, suggestive of alterations in myelin thickness between vehicle-treated WT and YAC128 HD mice (Fig. 4e; left panel; $p < 0.0001$). Whereas higher g-ratios were observed in callosal axons with an inner diameter below 0.5 μm in vehicle-treated YAC128 HD (Fig. 4e, left panel), suggesting thinner myelin sheaths compared with vehicle-treated WT mice, lower g-ratios were observed in callosal axons with an inner diameter above 0.5 μm (Fig. 4e, left panel), suggesting thicker or less compact myelin sheaths. These results were corroborated by the cumulative frequency of g-ratios that showed significant differences in g-ratios between vehicle-treated YAC128 HD mice and vehicle-treated WT mice in axons with an inner diameter below and above 0.5 μm (Fig. 4f; left and right panels; Kolmogorov-Smirnov test, $p < 0.001$). In contrast to the results observed in the anterior region of the CC, laquinimod treatment had a significant effect on myelin thickness in the posterior region. Treatment with both doses of laquinimod (0.25 and 1 mg/kg) significantly reversed changes in g-ratio, and therefore, the myelin thickness in callosal axons compared with vehicle-treated YAC128 HD mice (Fig. 4e; middle and right panels). An examination of the scatter plot analysis of laquinimod-treated YAC128 HD mice (0.25 and 1 mg/kg) compared with vehicle-treated YAC128 HD mice showed that the best-fit lines of both treatment groups (slope $_{[0.25\ \text{mg/kg laquinimod}]} = 0.2249 \pm 0.0067$; slope $_{[1\ \text{mg/kg laquinimod}]} = 0.2034 \pm 0.0080$) were different from that of the vehicle-treated YAC128 HD mice (slope = 0.1533 ± 0.0075; $p < 0.0001$) (Fig. 4e; middle and right panels), and closer to the best-fit line observed in the vehicle-treated WT mice (slope = 0.2687 ± 0.0077) (Fig. 4e; left panel). Indeed, cumulative frequency analysis indicates that the low dose of laquinimod significantly reversed the disease driven change in

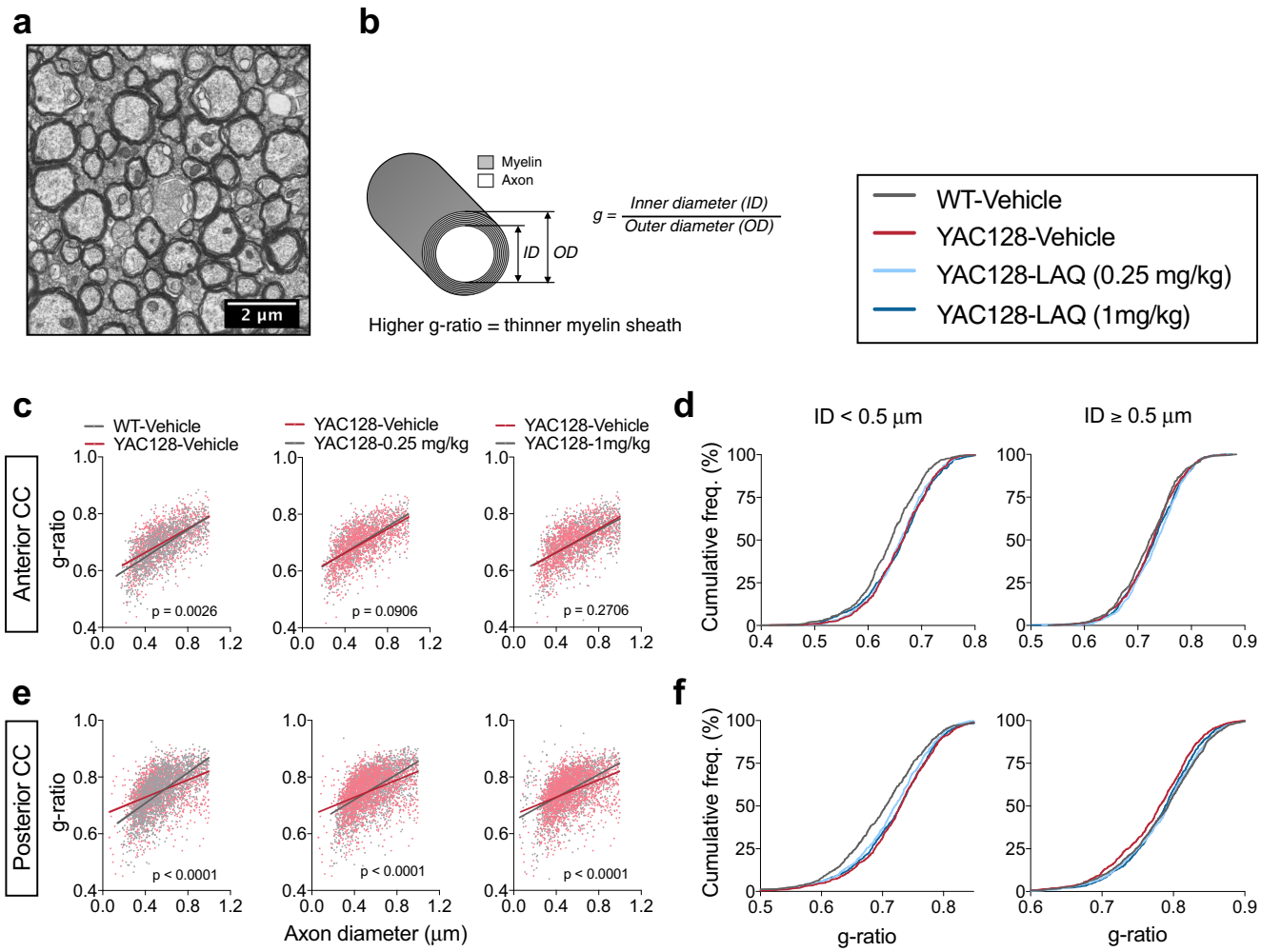

Fig. 4 Laquinimod reverses changes in myelin sheath thickness in the posterior region of the corpus callosum in YAC128 HD mice. Representative TEM image of callosal axons in the corpus callosum (CC) (**a**). Diagram representation of g-ratio measurement and calculation (axon diameter/outer diameter of the myelinated fibres) in myelinating axons (**b**). G-ratios shown as scattered plot against axon diameter with best vehicle-treated YAC128 vs low laquinimod-treated YAC128 ($p = 0.0906$) (**c**, middle panel), and vehicle-treated YAC128 vs high laquinimod-treated YAC128 ($p = 0.2706$) (**c**, right panel) in the anterior CC (**c**). Cumulative frequency analysis of g-ratios in axons with an inner diameter below and above 0.5 µm in the anterior region of the CC for all groups; Kolmogorov-Smirnov test ($p < 0.0001$ for vehicle-WT compared with vehicle-YAC128 HD mice in axons with ID < 0.5 µm; $p < 0.05$ for low laquinimod-YAC128 HD mice compared with vehicle-YAC128 HD mice in axons with ID ≥ 0.5 µm) (**d**). G-ratios shown as scattered plot against axon diameter with best-fit lines for vehicle-treated WT vs vehicle-treated YAC128 ($p < 0.0001$) (**e**, left panel), vehicle-treated YAC128 vs low laquinimod-treated YAC128 ($p < 0.0001$) (**e**, middle panel), and vehicle-treated YAC128 vs high laquinimod-treated YAC128 ($p < 0.0001$) (**e**, right panel) in the posterior CC (**e**). Cumulative frequency analysis of g-ratios in axons with an inner diameter below and above 0.5 µm in the posterior region of the CC for all groups; Kolmogorov-Smirnov test ($p < 0.0001$ for vehicle-WT compared with vehicle-YAC128 HD mice; $p < 0.01$ and $p < 0.001$ for low laquinimod-YAC128 HD mice compared with vehicle-YAC128 HD mice in axons with ID < 0.5 µm and ID ≥ 0.5 µm, respectively; $p < 0.01$ for high laquinimod-YAC128 HD mice compared with vehicle-YAC128 HD mice in axons with ID ≥ 0.5 µm) (**f**). Data represented as scatter plot of g-ratios against axonal diameter with best-fit line (**c**, **e**), and cumulative frequency of g-ratios (**d**, **f**); Kolmogorov-Smirnov test (**d**, **f**); $N = 4$ animals per genotype/group (all males); $N = 100$–600 axons per animals. Veh = vehicle; LAQ = laquinimod; CC = corpus callosum

g-ratios for axons with both an inner diameter below and above 0.5 µm compared with vehicle-treated YAC128 HD mice (Fig. 4f; left and right panels; Kolmogorov-Smirnov test, $p < 0.01$ for axons with a calibre below 0.5 µm and $p < 0.001$ for axons with a calibre above 0.5 µm), whereas the high dose of laquinimod only reversed g-ratios for axons with an inner diameter above 0.5 µm (Fig. 4f; left and right panels; Kolmogorov-Smirnov test, $p = 0.3603$ for axons with a calibre below 0.5 µm and $p < 0.01$ for axons with a calibre above 0.5 µm).

Altogether, our findings identify abnormal myelin sheath thickness in the anterior and posterior regions of the CC at 3 months of age in YAC128 HD mice, as previously described [27]. Notably, our results suggest that the improvements conferred by laquinimod treatment that were previously observed in magnetic resonance imaging-based measures of white

matter abnormalities in YAC128 HD mice [17] likely reflect laquinimod-mediated reversal of alterations in myelin sheath thickness, particularly in the posterior region of the CC.

Increased Levels of Myelin-Related Genes in the CC of Laquinimod-Treated YAC128 HD Mice

To understand whether the effect of laquinimod on myelin sheath thickness may be explained by changes at the molecular level, we investigated the expression levels of several myelin-related genes in the CC by quantitative real-time PCR (qRT-PCR). Vehicle-treated YAC128 HD mice showed significantly decreased levels of myelin basic protein (*Mbp*) compared with vehicle-treated WT mice (Fig. 5a; one-way ANOVA: $p = 0.0282$; Fisher's LSD post hoc analysis: $p > 0.05$; paired Student's *t* test: $p < 0.05$). However, no differences were observed in other myelin-related genes such as proteolipid protein 1 (*Plp1*) (Fig. 5b; one-way ANOVA: $p = 0.2471$), Ermin (*Ermn*) (Fig. 5c; one-way ANOVA: $p = 0.4366$), 2′,3′-cyclic nucleotide 3′ phosphodiesterase (*Cnp*) (Fig. 5d; one-way ANOVA: $p = 0.3641$) and myelin oligodendrocyte glycoprotein (*Mog*) (Fig. 5e; one-way ANOVA: $p = 0.4385$). *Mbp* transcript levels were significantly increased after treatment with either dose of laquinimod (Fig. 5a; one-way ANOVA: $p = 0.0282$; Fisher's LSD post hoc analysis: $p < 0.05$ for 0.25 mg/kg and $p < 0.01$ for 1 mg/kg of laquinimod); however, no effect of treatment was observed on other myelin-related genes investigated (Fig. 5b–e; one-way ANOVA: $p = 0.2471$ for *Plp1*, $p = 0.4366$ for *Ermn*, $p = 0.3641$ for *Cnp*, $p = 0.4385$ for *Mog*). To investigate whether the differences in *Mbp* transcript levels observed in the CC were paralleled by alterations in Mbp protein levels, we performed immunoblotting analysis for Mbp in the CC. Consistent with *Mbp* mRNA results, we observed lower levels of Mbp protein in the CC of vehicle-treated YAC128 HD mice compared with vehicle-treated WT mice (Fig. 5f), which were increased by both doses of laquinimod (Fig. 5f). These findings suggest that the increase in myelin thickness observed in laquinimod-treated YAC128 HD mice may be the result of laquinimod's action at the molecular level, rescuing Mbp mRNA and protein deficits in oligodendrocytes.

Effect of Laquinimod Treatment on Myelin- and Inflammation-Related Genes in the Striatum of YAC128 HD Mice

To further investigate the effect of laquinimod on myelin in other brain regions affected in HD, transcript levels of several myelin-related genes were assessed in the striatum by qRT-PCR. Vehicle-treated YAC128 HD mice showed decreased levels of *Mbp* and *Plp1* compared with vehicle-treated WT mice (Fig. 6a, b; one-way ANOVA: $p = 0.0017$ for *Mbp*, $p = 0.0217$ for *Plp1*; Fisher's LSD post hoc analysis: $p > 0.05$ for *Mbp*, $p < 0.01$ for *Plp;* paired Student's *t* test: $p < 0.05$ for *Mbp*). However, no differences were observed in other myelin-related genes such as *Ermn* (Fig. 6c; one-way ANOVA: $p = 0.7529$), *Cnp* (Fig. 6d; one-way ANOVA: $p = 0.4994$) and *Mog (*Fig. 6e; one-way ANOVA: $p = 0.3005$). *Mbp* transcript levels were significantly increased in a dose proportionate manner after treatment with laquinimod (Fig. 6a; one-way ANOVA: $p = 0.0017$; Fisher's LSD post hoc analysis: $p < 0.01$ for 0.25 mg/kg and $p < 0.001$ for 1 mg/kg of laquinimod), whereas *Plp1* transcript levels were increased only with the higher dose (Fig. 6b; one-way ANOVA: $p = 0.0217$; Fisher's LSD post hoc analysis: $p > 0.05$; paired Student's *t* test: $p < 0.05$) in YAC128 HD mice. Since laquinimod has been shown to exert immunomodulatory activity in both the periphery and the CNS, we also evaluated the effect of laquinimod on the inflammatory markers interleukin-6 (*Il6*), interleukin-1β (*Il1b*), and tumour necrosis factor alpha (*Tnfa*) by qRT-PCR in the striatum (Fig. 6f–h). At 3 months of age, no differences in expression levels of these genes were observed between any of the groups (Fig. 6f–h; one-way ANOVA: $p = 0.2012$ for *Il6*, $p = 0.9553$ for *Il1b*, $p = 0.4241$ for *Tnfa*), similar to the observations with glial cell densities (Fig. 3d–f). Altogether, these results suggest that the effects of laquinimod on myelin-related genes (*Mbp* and *Plp1*) are not limited to the CC, and that these effects are likely independent of its immunomodulatory effects.

Effect of Laquinimod on Cyp1A1, a Marker of AhR Activity, in YAC128 HD Mice

Laquinimod has recently been shown to induce expression of genes associated with the AhR pathway such as the Cytochrome P450 family 1 subfamily A member 1 (*Cyp1A1*) [14]. In order to examine whether the effects of laquinimod are mediated through AhR in the YAC128 HD mice, we measured the expression levels of *Cyp1A1* in the CC and striatum. In both brain regions, vehicle-treated YAC128 HD mice did not show differences in *Cyp1A1* expression levels compared with vehicle-treated WT mice (Supplementary Fig. S1a, b; one-way ANOVA: $p = 0.0160$ for CC, $p = 0.1565$ for striatum; Fisher's LSD post hoc analysis: $p > 0.05$ for CC and striatum; paired Student's *t* test: $p = 0.07$ for striatum). The high dose of laquinimod treatment (1 mg/kg) increased *Cyp1A1* levels in both the CC and striatum of YAC128 HD mice compared with vehicle-treated YAC128 HD mice and vehicle-treated WT mice, respectively (Supplementary Fig. S1a, b; one-way ANOVA: $p = 0.0160$ for CC, $p = 0.1565$ for striatum; Fisher's LSD post hoc analysis: $p < 0.01$ in the CC compared with vehicle-treated YAC128 HD mice, $p < 0.05$ in the striatum compared with vehicle-treated WT mice). However, the low dose of laquinimod treatment (0.25 mg/kg) had no effect on *Cyp1A1* levels (Supplementary Fig. S1a, b; one-way ANOVA: $p = 0.0160$ for CC, $p = 0.1565$ for striatum; Fisher's LSD post hoc analysis: $p > 0.05$ for CC and striatum).

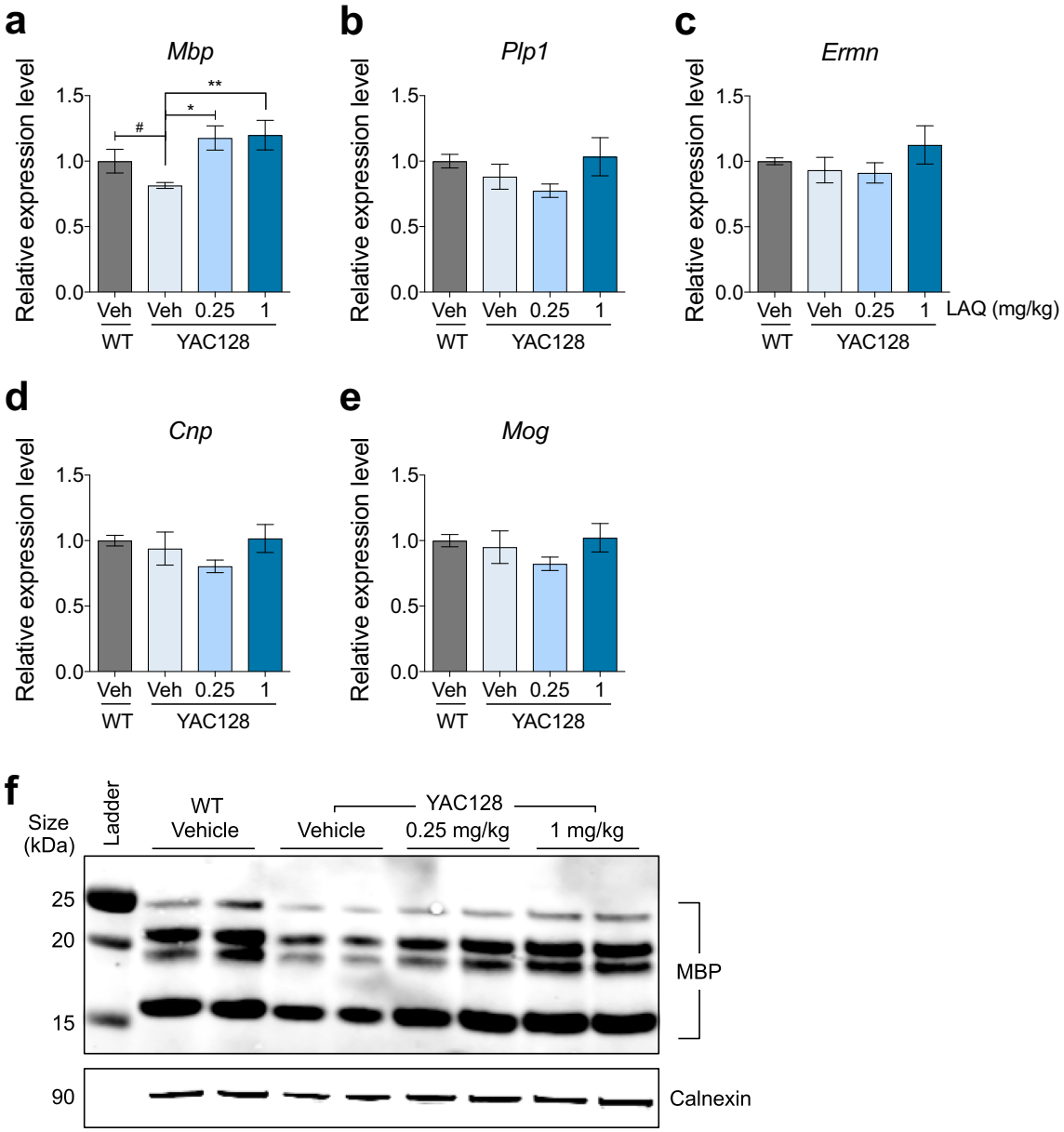

Fig. 5 Effect of laquinimod treatment on myelin-related genes in the corpus callosum of YAC128 HD mice. Vehicle-treated YAC128 HD mice showed *Mbp* transcriptional deficits in the corpus callosum of YAC128 HD mice (**a**), but no differences were observed in other myelin-related genes including *Plp1* (**b**), *Ermn* (**c**), *Cnp* (**d**) *and Mog* (**e**). Laquinimod treatment (0.25 and 1 mg/kg) only rescued *Mbp* transcriptional deficits in YAC128 HD mice (**a**) but no effect was observed in the other myelin-related genes (**b**–**e**). Vehicle-treated YAC128 HD mice showed decreased Mbp protein levels in the corpus callosum compared with vehicle-treated WT mice, which were increased by both doses of laquinimod (**f**). Values shown as mean ± SEM; $*p < 0.05$, $**p < 0.01$ by one-way ANOVA with Fisher's LSD post hoc analysis; $^{\#}p < 0.05$, by paired Student's *t* test; $N = 6$ per genotype/group (all males) for **a**–**e**; Veh = vehicle; LAQ = laquinimod; *Mbp* = myelin basic protein; *Plp1* = proteolipid protein 1; *Ermn* = Ermin; *Cnp* = 2′,3′-cyclic nucleotide 3′ phosphodiesterase; *Mog* = myelin oligodendrocyte glycoprotein; kDa = kilodaltons

Altogether, our data shows *Cyp1A1* induction by the higher dose of laquinimod in the CC supporting engagement of the AhR pathway at this dose. However, the low dose of laquinimod did not induce *Cyp1A1* in any of the brain regions investigated, suggesting that the improvements seen with the administration of the lower dose of laquinimod may be mediated by an AhR-independent mechanism.

Discussion

Several studies have shown laquinimod's beneficial effects in animal models of MS to be related to its immunomodulatory activity and mediated largely via AhR activation [14, 15]. Much less is known about the mechanism(s) of action of laquinimod in HD where we and others have shown it to

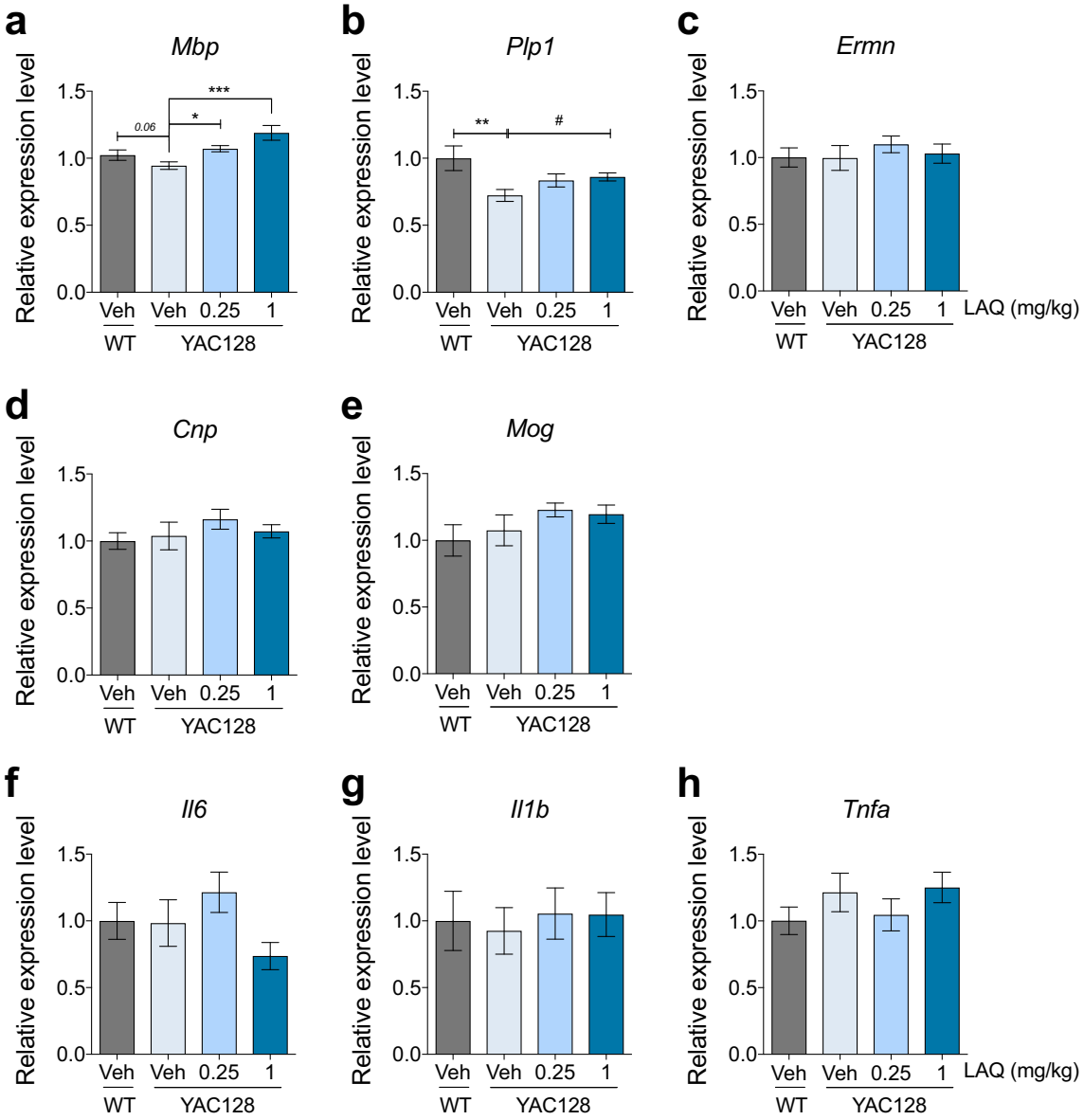

Fig. 6 Effect of laquinimod treatment on myelin-related and inflammatory genes in the striatum of YAC128 HD mice. Vehicle-treated YAC128 HD mice showed *Mbp* (**a**) and *Plp1* (**b**) transcriptional deficits in the striatum of YAC128 HD mice at 3 months of age, but no differences were observed in other myelin-related genes including, *Ermn* (**c**), *Cnp* (**d**) *and Mog* (**e**). Whereas laquinimod treatment (0.25 and 1 mg/kg) rescued *Mbp* transcriptional deficits in the striatum of YAC128 HD mice (**a**), only the high dose of laquinimod rescued *Plp1* transcriptional deficits (**b**). No effect of laquinimod treatment was observed in the other myelin-related genes (**b**–**e**). At 3 months of age, no differences in inflammatory-related genes such as *Il6* (**f**), *Il1b* (**g**) and *Tnfa* (**h**) were observed between groups. Values shown as mean ± SEM; $^{*}p < 0.05$, $^{**}p < 0.01$, $^{***}p < 0.001$ by one-way ANOVA with Fisher's LSD post hoc analysis; $p = 0.06$, $^{\#}p < 0.05$ by paired Student's *t* test; N = 6 per genotype/group (all males). Veh = vehicle; LAQ = laquinimod; *Mbp* = myelin basic protein; *Plp1* = proteolipid protein 1; *Ermn* = Ermin; *Cnp* = 2′,3′-cyclic nucleotide 3′ phosphodiesterase; *Mog* = myelin oligodendrocyte glycoprotein; *Il6* = interleukin-6; *Il1b* = interleukin-1β; *Tnfa* = tumour necrosis factor alpha

improve a number of behavioural and pathological aspects of the disease, including white matter deficits [17, 29, 30]. In this study, we explored the effects of laquinimod on white matter at the cellular, molecular and ultrastructural levels. We first show that early treatment with laquinimod improves motor learning, and confirm its antidepressant properties. We then demonstrate, for the first time, that laquinimod reverses changes in myelin sheath thickness observed in the CC of YAC128 HD mice, which is accompanied by an increase in expression levels of *Mbp*. Our findings suggest that the beneficial effects of laquinimod on white matter microstructural abnormalities in HD may be independent of its AhR-mediated immunomodulatory activity.

We previously showed that laquinimod treatment (1 and 10 mg/kg) resulted in behavioural improvements in YAC128 HD mice [17]. In this study, we explored whether lowering the

dose of laquinimod further to 0.25 mg/kg could also improve HD-related phenotypes. We evaluated the effect of laquinimod on cognitive function for the first time and found modest improvements in motor learning using the rotarod task. We also found a very striking effect of laquinimod on depressive behaviour in YAC128 mice, even at the lowest dose used (0.25 mg/kg). However, laquinimod did not improve motor deficits in the accelerating rotarod in YAC128 HD mice at 3 months of age, which is consistent with our previous findings showing the earliest improvements of motor deficits by laquinimod at 4 months of age [17]. These findings support the use of laquinimod for the treatment of certain manifestations of HD, and in particular depression, and also indicate that a reduced dose of laquinimod (0.25 mg/kg) can exert similar beneficial effects as observed with a higher dose (1 mg/kg).

Deficits in motor learning have been described to first manifest at 2 months of age in YAC128 HD mice using the rotarod task [25]. In this study we show that early administration of laquinimod prior the appearance of disease phenotypes (5 weeks of age) can lead to motor learning improvements, suggesting that early treatment may be important to delay the appearance of HD-related disease phenotypes. Another notable aspect of the current study design is the short treatment period (7 weeks here versus 6 months in our previous study [17]). Interestingly and despite the short period of laquinimod treatment, we observed improvements in several HD-related phenotypes in YAC128 HD mice. Whether the beneficial effects of 7 weeks of treatment with laquinimod would persist after treatment cessation or would require continued administration remains to be determined.

A primary goal of the present study was to investigate the nature of the WM improvements identified by diffusion tensor imaging in laquinimod-treated YAC128 HD mice [17]. Our observations of no changes in oligodendroglial population densities in the YAC128 mice at 3 months, with or without laquinimod treatment, suggest that the improvements in WM alterations are likely mediated by cell intrinsic effects. Furthermore, the lack of effect on glial populations (astrocytes and microglia) previously implicated in laquinimod's immunomodulatory activity [33] also suggests that the white matter improvements in young YAC128 mice observed may be independent of immune modulation.

Studies in rodent models of HD have shown that WM-related microstructural abnormalities are an early feature of the disease, and involve thinner myelin sheaths and reduced myelin-related genes expression in the CC [27, 31, 32]. Using TEM analysis, we show that YAC128 HD mice have thinner myelin sheaths at 3 months of age in the anterior region of the CC as we previously reported [27]. We further describe, for the first time, differences at the ultrastructural level in myelin sheaths in the posterior region of the CC. Interestingly, these differences consisted of thinner myelin sheaths in axons with a calibre below 0.5 μm, as seen in the anterior region, and thicker myelin sheaths in axons with a calibre above 0.5 μm. Furthermore, we showed that laquinimod treatment reversed myelin sheath thickness only in axons from the posterior region of the CC in YAC128 HD mice, findings that parallel the improvements in fractional anisotropy observed only in the posterior region of the CC in laquinimod-treated YAC128 HD mice in our previous study [17]. Altogether, the results suggest a region-specific effect of laquinimod on WM ultrastructure.

While these differences in myelin sheath thickness in the posterior region of the CC in YAC128 HD mice cannot be explained by changes in the density of glial populations, they may be related to changes in the expression of myelin-related genes. As previously shown in R6/2 mice [31] and in primary OPC-differentiated oligodendrocytes obtained from YAC128 HD mice [27], we also found decreased *Mbp* transcript and protein levels in the CC of YAC128 HD mice, which were rescued by laquinimod treatment. Similar rescue of *Mbp* transcript levels was observed in the striatum of YAC128 HD mice, where deficits in *Plp1* transcript levels were also reversed. Interestingly, the laquinimod treatment appears to affect primarily expression levels of components of compact myelin (MBP and PLP), and not non-compact myelin (CNP, MOG and Ermin) [33, 34]. These findings point to the possibility that the thinning and decompaction of myelin seen in HD [27, 31] may be related to deficits in protein determinants of myelin compaction such as MBP and PLP [33, 34], and that the beneficial effects of laquinimod on white matter and myelination in HD is partly due to reversal of these deficits in compact myelin components.

While the focus of the present study was to evaluate the efficacy of laquinimod in reversing HD-related white matter pathology, it would be interesting to investigate in future studies how laquinimod might affect oligodendroglia and myelination under normal physiological conditions.

Laquinimod has been shown to mediate its immunomodulatory response through the AhR pathway and to induce genes associated to AhR activation such as the *Cyp1A1* [14]. In our study, we observed induction of *Cyp1A1* with the high dose of laquinimod (1 mg/kg) only, with no effect on expression levels of inflammatory factors. Taken together with the improvements in WM and myelination seen with the low dose (0.25 mg/kg) where no upregulation of *Cyp1A1* was observed, these results suggest that laquinimod's effect on myelination in this dose range may be independent of AhR activation. Nonetheless, a role for AhR cannot be formally excluded given reports of a possible role for AhR in the regulation of myelination [35] based on studies in AhR knockout (AhR KO) animals [35]. AhR KO mice display thinner myelin sheaths in the sciatic nerve fibres along with dysregulation of the expression myelin genes as well as myelin developmental markers [35]. Future studies are warranted to delineate the role of AhR in mediating the effects of laquinimod on white matter pathology and myelination deficits in HD.

Overall, our study demonstrates that laquinimod treatment improves a number of HD-related myelination abnormalities by modulating the expression of compact myelin-related genes in oligodendrocytes and reversing ultrastructural changes in myelin sheaths in YAC128 HD mice. Our results support further investigation of laquinimod as therapeutic intervention to tackle WM abnormalities in HD.

Acknowledgements Microscopy images for this study were acquired at the SBIC-Nikon Imaging Centre (Biopolis, Singapore).

Author Contributions M.G.M. designed and performed experiments, data analysis and interpretation, and wrote the manuscript. N.A.B.M.Y., J.Y.T., C.R., H.S. and L.J.T. performed experiments. N.Z. and M.R.H. contributed to the study design and revision of the manuscript. M.A.P. conceived and designed experiments, participated in analysis and interpretation of data, and wrote the manuscript.

Funding Information This study was supported by a grant from Teva Pharmaceuticals. M.A.P. is supported by a Strategic Positioning Fund for Genetic Orphan Diseases (SPF2012/005) from the Agency for Science Technology and Research, and by the National University of Singapore, Singapore.

Compliance with Ethical Standards

Conflict of Interest N.Z., H.B. and M.R.H. are employees of Teva Pharmaceuticals, and contributed to the study design and revision of the manuscript. Teva Pharmaceuticals played no role in the treatment or testing of animals, or the collection, analysis and interpretation of the results.

References

1. Bates GP, Dorsey R, Gusella JF, Hayden MR, Kay C, Leavitt BR, Nance M, Ross CA, et al. (2015) Huntington disease. Nat Rev Dis Primers 15005. doi: https://doi.org/10.1038/nrdp.2015.5
2. Tai YF, Pavese N, Gerhard A, Tabrizi SJ, Barker RA, Brooks DJ, Piccini P (2007) Microglial activation in presymptomatic Huntington's disease gene carriers. Brain 130:1759–1766. https://doi.org/10.1093/brain/awm044
3. Andre R, Carty L, Tabrizi SJ (2015) Disruption of immune cell function by mutant huntingtin in Huntington's disease pathogenesis. Curr Opin Pharmacol 26:33–38. https://doi.org/10.1016/j.coph.2015.09.008
4. Crotti A, Glass CK (2015) The choreography of neuroinflammation in Huntington's disease. Trends Immunol 36:364–373. https://doi.org/10.1016/j.it.2015.04.007
5. Denis HL, Lauruol F, Cicchetti F (2018) Are immunotherapies for Huntington's disease a realistic option? Mol Psychiatry 16:889. https://doi.org/10.1038/s41380-018-0021-9
6. Sapp E, Kegel KB, Aronin N, Hashikawa T, Uchiyama Y, Tohyama K, Bhide PG, Vonsattel JP et al (2001) Early and progressive accumulation of reactive microglia in the Huntington disease brain. J Neuropathol Exp Neurol 60:161–172
7. Pavese N, Gerhard A, Tai YF, Ho AK, Turkheimer F, Barker RA, Brooks DJ, Piccini P (2006) Microglial activation correlates with severity in Huntington disease: a clinical and PET study. Neurology 66:1638–1643. https://doi.org/10.1212/01.wnl.0000222734.56412.17
8. Björkqvist M, Wild EJ, Thiele J, Silvestroni A, Andre R, Lahiri N, Raibon E, Lee RV et al (2008) A novel pathogenic pathway of immune activation detectable before clinical onset in Huntington's disease. J Exp Med 205:1869–1877. https://doi.org/10.1084/jem.20080178
9. Politis M, Pavese N, Tai YF, Kiferle L, Mason SL, Brooks DJ, Tabrizi SJ, Barker RA et al (2011) Microglial activation in regions related to cognitive function predicts disease onset in Huntington's disease: a multimodal imaging study. Hum Brain Mapp 32:258–270. https://doi.org/10.1002/hbm.21008
10. Politis M, Lahiri N, Niccolini F, Su P, Wu K, Giannetti P, Scahill RI, Turkheimer FE et al (2015) Increased central microglial activation associated with peripheral cytokine levels in premanifest Huntington's disease gene carriers. Neurobiol Dis 83:115–121. https://doi.org/10.1016/j.nbd.2015.08.011
11. Wild E, Magnusson A, Lahiri N, Krus U, Orth M, Tabrizi SJ, Björkqvist M (2011) Abnormal peripheral chemokine profile in Huntington's disease. PLoS Curr 3:RRN1231. https://doi.org/10.1371/currents.RRN1231
12. Weiss A, Träger U, Wild EJ, Grueninger S, Farmer R, Landles C, Scahill RI, Lahiri N et al (2012) Mutant huntingtin fragmentation in immune cells tracks Huntington's disease progression. J Clin Invest 122:3731–3736. https://doi.org/10.1172/JCI64565
13. Varrin-Doyer M, Zamvil SS, Schulze-Topphoff U (2014) Laquinimod, an up-and-coming immunomodulatory agent for treatment of multiple sclerosis. Exp Neurol 262PA:66–71. https://doi.org/10.1016/j.expneurol.2014.04.002
14. Kaye J, Piryatinsky V, Birnberg T, Hingaly T, Raymond E, Kashi R, Amit-Romach E, Caballero IS et al (2016) Laquinimod arrests experimental autoimmune encephalomyelitis by activating the aryl hydrocarbon receptor. PNAS 113:E6145–E6152. https://doi.org/10.1073/pnas.1607843113
15. Aharoni R, Saada R, Eilam R, Hayardeny L, Sela M, Arnon R (2012) Oral treatment with laquinimod augments regulatory T-cells and brain-derived neurotrophic factor expression and reduces injury in the CNS of mice with experimental autoimmune encephalomyelitis. J Neuroimmunol 251:14–24. https://doi.org/10.1016/j.jneuroim.2012.06.005
16. Thöne J, Ellrichmann G, Seubert S, Peruga I, Lee DH, Conrad R, Hayardeny L, Comi G et al (2012) Modulation of autoimmune demyelination by laquinimod via induction of brain-derived neurotrophic factor. Am J Pathol 180:267–274. https://doi.org/10.1016/j.ajpath.2011.09.037
17. Garcia-Miralles M, Hong X, Tan LJ, Caron NS, Huang Y, To XV, Lin RY, Franciosi S et al (2016) Laquinimod rescues striatal, cortical and white matter pathology and results in modest behavioural improvements in the YAC128 model of Huntington disease. Sci Rep 6:31652. https://doi.org/10.1038/srep31652
18. Garcia-Miralles M, Geva M, Tan JY, Yusof NABM, Cha Y, Kusko R, Tan LJ, Xu X et al (2017) Early pridopidine treatment improves behavioral and transcriptional deficits in YAC128 Huntington disease mice. JCI Insight 2. https://doi.org/10.1172/jci.insight.95665
19. Brooks SP, Dunnett SB (2009) Tests to assess motor phenotype in mice: a user's guide. Nat Rev Neurosci 10:519–529. https://doi.org/10.1038/nrn2652
20. Pouladi MA, Graham RK, Karasinska JM, Xie Y, Santos RD, Petersen A, Hayden MR (2009) Prevention of depressive behaviour in the YAC128 mouse model of Huntington disease by mutation at residue 586 of huntingtin. Brain 132:919–932. https://doi.org/10.1093/brain/awp006
21. Paxinos G, Franklin KB (2012) Paxinos and franklin's the mouse brain in stereotaxic coordinates. Academic Press
22. Barazany D, Basser PJ, Assaf Y (2009) In vivo measurement of axon diameter distribution in the corpus callosum of rat brain. Brain 132(5):1210–1220

23. Pouladi MA, Stanek LM, Xie Y, Franciosi S, Southwell AL, Deng Y, Butland S, Zhang W et al (2012) Marked differences in neurochemistry and aggregates despite similar behavioural and neuropathological features of Huntington disease in the full-length BACHD and YAC128 mice. Hum Mol Genet 21:2219–2232. https://doi.org/10.1093/hmg/dds037
24. Van Raamsdonk JM, Murphy Z, Slow EJ, Leavitt BR, Hayden MR (2005) Selective degeneration and nuclear localization of mutant huntingtin in the YAC128 mouse model of Huntington disease. Hum Mol Genet 14:3823–3835. https://doi.org/10.1093/hmg/ddi407
25. Van Raamsdonk JM, Pearson J, Slow EJ, Hossain SM, Leavitt BR, Hayden MR et al (2005) Cognitive dysfunction precedes neuropathology and motor abnormalities in the YAC128 mouse model of Huntington's disease. J Neurosci 25:4169–4180. https://doi.org/10.1523/JNEUROSCI.0590-05.2005
26. Carroll JB, Lerch JP, Franciosi S, Spreeuw A, Bissada N, Henkelman RM, Hayden MR (2011) Natural history of disease in the YAC128 mouse reveals a discrete signature of pathology in Huntington disease. Neurobiol Dis 43:257–265. https://doi.org/10.1016/j.nbd.2011.03.018
27. Teo RTY, Hong X, Yu-Taeger L, Huang Y, Tan LJ, Xie Y, To XV, Guo L et al (2016) Structural and molecular myelination deficits occur prior to neuronal loss in the YAC128 and BACHD models of Huntington disease. Hum Mol Genet 25:2621–2632. https://doi.org/10.1093/hmg/ddw122
28. Brück W, Pförtner R, Pham T, Zhang J, Hayardeny L, Piryatinsky V et al. (2012) Reduced astrocytic NF-κB activation by laquinimod protects from cuprizone-induced demyelination. Acta Neuropathologica 124(3):411–424. https://doi.org/10.1007/s00401-012-1009-1
29. Zwilling D, Huang S-Y, Sathyasaikumar KV, Notarangelo FM, Guidetti P, Wu HQ, Lee J, Truong J et al (2011) Kynurenine 3-monooxygenase inhibition in blood ameliorates neurodegeneration. Cell 145:863–874. https://doi.org/10.1016/j.cell.2011.05.020
30. Ehrnhoefer DE, Caron NS, Deng Y, Qiu X, Tsang M, Hayden MR (2016) Laquinimod decreases Bax expression and reduces caspase-6 activation in neurons. Exp Neurol 283:121–128. https://doi.org/10.1016/j.expneurol.2016.06.008
31. Xiang Z, Valenza M, Cui L, Leoni V, Jeong HK, Brilli E, Zhang J, Peng Q et al (2011) Peroxisome-proliferator-activated receptor gamma coactivator 1 α contributes to dysmyelination in experimental models of Huntington's disease. J Neurosci 31:9544–9553. https://doi.org/10.1523/JNEUROSCI.1291-11.2011
32. Jin J, Peng Q, Hou Z, Jiang M, Wang X, Langseth AJ, Tao M, Barker PB et al (2015) Early white matter abnormalities, progressive brain pathology and motor deficits in a novel knock-in mouse model of Huntington's disease. Hum Mol Genet 24:2508–2527. https://doi.org/10.1093/hmg/ddv016
33. Baumann N, Pham-Dinh D (2001) Biology of oligodendrocyte and myelin in the mammalian central nervous system. Physiol Rev 81:871–927
34. Jahn O, Tenzer S, Werner HB (2009) Myelin proteomics: molecular anatomy of an insulating sheath. Mol Neurobiol 40:55–72. https://doi.org/10.1007/s12035-009-8071-2
35. Shackleford G, Sampathkumar NK, Hichor M et al (2018) Involvement of Aryl hydrocarbon receptor in myelination and in human nerve sheath tumorigenesis. PNAS 115:E1319–E1328. https://doi.org/10.1073/pnas.1715999115